OBJECT CONTOUR EXTRACTION BASED ON CHARGED SNAKE MODEL

MAN LIU

Object Contour Extraction Based on Charged Snake Model

by

© Man Liu

A thesis submitted to the

School of Graduate Studies

in partial fulfillment of the

requirements for the degree of

Master of Science

Department of Computer Science

Memorial University of Newfoundland

April 2011

St. John's Newfoundland

Abstract

The active contour model, or snake, is one of the most successful variational models in image extraction and segmentation. In this thesis, a novel Charged Snake Model (CSM), based on electrostatic theory for object contour extraction is proposed. This method overcomes several difficulties existing in conventional parametric snake models. A closed contour locates the initial contour of the snake and each point in the initial snake contour is regarded as a charge, which makes the initial CSM snake close enough to the object boundary to allow for faster convergence. Furthermore, due to the interaction among all charges in the snake, the snake model is not sensitive to and is not influenced by the initialization position. As for CSM snake, an improved and associated energy function, with employing additional parameters, is generated. Under the influence of internal and external image dependent forces, the initial CSM snake deforms towards the minimum of the energy function where the object boundary is located and the CSM snake reaches its convergence. By this process, a complete object shape, as well as the object position described by the CSM snake, can be obtained. This shape and position information can then be used in further shape analysis.

Acknowledgments

I want to thank my supervisor, Dr. Siwei Lu, for his insightful guidance, constructive suggestion and patience. Without his help, it would not have been possible to finish this thesis, and certainly not at its current level of quality.

I would like to acknowledge the financial support received from the Department of Computer Science.

I am very grateful to the administrative staff. Elaine Boone and all of the department's secretaries have helped me a great deal in the preparation of this thesis.

I would like to thank system support staff for providing all the help and assistance during my research.

In addition, special thanks go to Dr. Minglun Gong for helping me with the thesis correction.

Finally, I would like to thank my fellow graduate students, and in particular to Grant Strong, Tao Chen and Zheng Chen for their assistance and encouragement during the research and preparation of the thesis.

Contents

List of Tables

List of Figures

Chapter 1 Introduction

The earliest and best known active contour approach is *snakes*, which are considered to be deformable splines. The splines are acted upon by image, internal and user-defined "forces", thereby deforming to minimize the "energy" resisting these forces. Snake, or active contour, was originally developed by M. Kass [1] in 1987. The problem of extracting the image contours is transformed into the problem of minimizing the energy by this method. A curve constrained by a set of parameters is moved actively toward the image contours under internal, external, and constrained forces. The curve is converged at the edge of the image contours when its energy is minimal. The global information of the image contours is used to get a close curve and any prior knowledge about the image is not necessary; therefore, it has a successfully broad application in a variety of problems in computer vision and image analysis, such as edge and subjective contours detection, image segmentation, motion tracking [2].

The Snake Model is driven by the potential energy generated by processing an image. Tension and stiffness forces keep the boundary of the model smooth, and a pressure force can be added so that closed models expand like balloons. Snake models also have been widely used in traffic management [59], surveillance and robotics [60]. This type of technique has been used successfully for tracking the movement of lips in a computerized lip-reading application, and for tracking the movements of objects in medical images [3].

Furthermore, another main contribution coming from snake applications is for processing the medical image. There are a great amount of uses in computed tomography (CT) and magnetic resonance (MR) image analysis, and many medial image analysis applications [10, 61], such as the measurement of anatomical structures, require prior extraction of the organ from the surrounding tissue. However, the traditional snakes have a lot of weaknesses such as the snakes are highly sensitive to their initial contours. Thereby the initial contours must be close to the real image contours [42], otherwise snakes would finally deform to an incorrect result. Also, another difficulty coming from the traditional snakes is to converge into the deep concave boundary. Additionally, slow convergence speed, partial convergence incidental to the result and sensitive to noise are also the drawbacks of the traditional snakes. Aimed at these defects, many improvement methods have been presented. In general, each of these methods is created by building a new external force. These methods include pressure forces [14], distance potentials [9], gradient vector flow snake [23] and other methods with building a new external force. All of these methods have a large capture range; hence, the initial contours do not need to be near the real image contours anymore [42]. However, additional defects are seen for these methods: pressure forces can push an active contour go through, namely failure at, the object boundary if edges of the object are unobvious. Furthermore, weakness of the failure of converging into a deep concave boundary still exists in these methods. The GVF [23] snake has obvious weaknesses which include high computational cost, noise sensitivity, parameter sensitivity, and the ambiguous relationship between the capture range and parameters [46].

Aimed at the weaknesses of the traditional snake and the defects of the above improvement methods, a snake model based on the static electric field is presented. This snake model possesses a very large capture range and no difficultly converges into a deep concave boundary. In contrast to other snake models based on the static electric field, our snake model is not restricted by initialization position due to interaction among charges in the snake; furthermore, the snake model is easier to converge into a deep concave C-shape boundary via adjusting the additional parameters in normal formulae.

1.1 Proposed Snake Model

All aforementioned deformable models employ energy-based [1,13,14], or geometric-based, minimization approaches [15,16,17] that evolve an initial curve under the influence of external potentials, while the curve is being constrained by internal energies. Snakes are usually parameterized (using B-splines) and the solution space is constrained to have a predefined shape [13,18,19]. These methods require an accurate initialization step, since the initial contour converges iteratively towards the solution of a partial differential equation.

In our work, a novel snake model, based on charged particles, is proposed. Each point in the snake is regarded as a charge. All charges are attracted towards the contours of the objects of interest by an electric field [58], whose sources are computed based on the gradient magnitude. The electric field plays the same role as the potential force in the snake model, while internal interactions are modeled by repulsive electrostatic forces. In contrast to attractive forces based on the gradient-magnitude [1], the attractive forces act only along boundaries of objects; the electric field exhibits increased capture range because of its long range attraction and enhanced robustness against boundary leakage. Due to the combined effect of the internal energy of snake, external interactions of charges with the electrostatic field, and repelling forces between charges in the snake, the snake converge without difficulty into deep boundary concavities or internal boundaries separating embedded objects. Moreover, the method is insensitive to initialization and can achieve object contour extraction and shape segmentation as well.

Our system works on the following process: the location of the object shape can be estimated. Then, the edge map of the object is obtained from the original image. A thinning algorithm is then applied to the edges. Finally, the new Charged Snake Model (CSM) snake is used for the object boundary-tracing task.

1.2 Organization of this Thesis

This thesis is organized into six chapters. In Chapter Two, a review on traditional parametric snakes is presented. In Chapter Three, a new snake design is proposed, which overcomes some difficulties of traditional snakes. Following this, the entire motion tracking stages with the new snake are demonstrated in Chapter Four. The experiment on the new snake is given in Chapter Five. Finally, a conclusion is drawn in Chapter Six.

Chapter 2 Survey of Active Contour Models (Snakes)

In the past more than twenty of years, there have been increasing interests in the research of active contour model due to its wide applications in image processing field. Various snakes were designed for their own applications. Snakes are involved in many computer vision applications, including segmentation [19], edge detection [1], motion tracking [21] and shape modeling [22]. Each snake has its own advantages and disadvantages. These characteristics make snakes perform perfectly in specific applications but not sufficiently in others. The following section of this chapter investigates different types of snake model designs and categorizes them based on their main characteristics.

2.1 The Background of Snake Models

The snake algorithm was essentially just the minimization of an energy function which depends on the snake's position and attributes of the image (typically the position of edges as determined by the magnitude of the image gradient). In the original snake formulation of Kass *et al.* [1,24], the best snake position was defined as the solution of a variational problem requiring the minimization of the sum of internal and external energies integrated along the length of the snake. Thereafter, many approaches such as balloon snake [13,14], GVF snakes, SSEF snake, geometric snake and geodesic snake were successfully researched and developed and contributed to the image processing field [43,44,45].

Rather than the research being conducted on applications of snakes, another class of research focused on the reformulation of both the internal forces [38] and image forces [39] and the representation of the contour [40]. The main objective of this class of research was to minimize the amount of user intervention needed to obtain robust performance [41].

2.1.1 Traditional Snakes

Active contours, *snakes*, or *deformable models*, were self deforming dynamic curves defined within an image space, which can move under the influence of internal forces within the curve itself and external forces derived from specified image data [1,23]. The internal and external forces were defined so that the snake would move to an object boundary or other desired features within an image.

Deformable models largely fell under two major categories: *parametric deformable models* [1,14] and *geometric deformable models* [17]. The parametric deformable models represented deformable curves and surfaces in their parametric forms. And the geometric deformable models represented curves and surfaces implicitly as a level set of a higher-dimensional scalar function. In this chapter, the *parametric deformable models* would be focused on because the proposed model fell into this category. Therefore, the terms *snake* and *active contour* referred to parametric deformable models in the following sections unless specified otherwise.

2.2 Parametric Deformable Models

Parametric deformable models consisted basically of an elastic curve (or surface), which could dynamically conform to object shapes in response to internal forces (elastic forces) and external forces (image and constraint forces). These forces were the result of a functional global minimization process based on local information. Such an approach was more intuitive than the implicit models. Its mathematical formulation made it easier to integrate image data, an initial position estimated, desired contour properties and knowledge-based constraints, in a single extraction process [5].

Almost all of these snakes differed in the second term, namely external energy function, in the energy function [1]. Different designs for external energy function were able to build up their own snakes with some advantages and disadvantages. In the following parts of this section, a few different external forces would be introduced.

2.2.1 Multiscale Gaussian Potential Force

Given an image $I(x, y)$, the external energies designed to lead an active contour toward step edges are:

$$E_{ext}^{(1)}(x, y) = -\left|grad(I(x, y))\right|^2 \qquad (2.1)$$

$$E_{ext}^{(2)}(x,y) = -\left|grad\left(G_\sigma(x,y) * I(x,y)\right)\right|^2 \qquad (2.2)$$

where $G_\sigma(x,y)$ was a two-dimensional Gaussian function with standard deviation σ, and *grad*() was the gradient operator. $*$ was the convolution operator. σ had to be selected to have a small value in order to follow the boundary accurately. As a result, the Gaussian potential force was only able to attract the model toward the boundary when it was initialized nearby. To remedy this problem, Terzopoulos, Witkin, and Kass [1,24] applied Gaussian potential forces at different scales to broaden its attraction range while maintaining the model's boundary localization accuracy (A wavelet transformation was able to be used to obtain a set of multiscale images). At first, a large value σ was used to create a potential energy function with a broad valley around the boundary. The coarse-scale Gaussian potential force attracted the deformable contour or surface toward the desired boundaries from a long range. When the contour or surface reached equilibrium, the value of σ was then reduced to allow tracking of the boundary at a finer scale. This scheme effectively extended the attraction range of the Gaussian potential force. A weakness of this approach, however, is no established theorem for scheduling changes in σ. The available specified scheduling schemes may therefore lead to unreliable results.

2.2.2 Pressure Force

Cohen [19] proposed to increase the attraction range by using a pressure force together with the Gaussian potential force. The pressure force was able to either inflate or deflate the model; hence, it removed the requirement to initialize the model near the desired object boundaries. Deformable models that used pressure forces were also known as balloons [13,14].

The pressure force was defined as

$$F_p(X) = \omega_p N(X) \tag{2.3}$$

where $N(X)$ was the inward unit normal for the model at the point X and ω_p was a weighting parameter. The sign of ω_p determined whether to inflate or deflate the model and was typically chosen by users. Recently, region information has been used to define ω_p with a spatial-varying sign based upon whether the model was inside or outside the desired object [25]. The value of ω_p determined the strength of the pressure force. It must be carefully selected so that the pressure force was slightly smaller than the Gaussian potential force at edges, but large enough to pass through weak or spurious edges. When the model deformed, the pressure force kept inflating or deflating the model until the Gaussian potential force stops it. A disadvantage in using pressure forces was that they may cause the deformable model to cross itself and form a small dot [26].

2.2.3 Gradient Vector Flow Snake

Xu and Prince suggested [23] that there were two important problems with the snake work. The problems were *Capture Range problem* and *Concavity problem*, which caused that the snake unable to progress into the deep concave. However, the Gradient vector flow (GVF) snake proposed by Xu and Prince was able to solve the two problems. They employed a vector diffusion equation from the classical smoothing constraint in optical flow (Horn and Schunck [27]), thus the gradient of an edge map was diffused in regions distant from the boundary; thereby a different force field (GVF field) was yielded. The amount of diffusion was adapted according to the strength of edges to avoid distorting object boundaries.

GVF, is an external force defined as $V(x,y)=(u(x,y),v(x,y))$ which minimized the energy function

$$\varepsilon = \iint \mu\left(u_x^2+u_y^2+v_x^2+v_y^2\right)+\left|\nabla f\right|^2\left|V-\nabla f\right|^2 dxdy \tag{2.4}$$

This variational formulation followed a standard principle, that of making the result smooth when there was no data. Where $f(x,y)=-E_{ext}(x,y)$ was an edge map derived from the image $I(x,y)$, having the property that it was larger near the image edge. After $V(x,y)$was computed, the potential force $-\nabla E_{ext}$ in basic energy function was applied. GVF had a large attraction range and improved convergence for deforming contours into boundary concavities [23].

Although GVF snake had an improvement in those two raised problems, in fact it was still not able to solve the concavity problem perfectly. Xu and Prince stated that the GVF snake still had difficulties forcing a snake into long, thin boundary concavities. Additionally, the GVF snake was sensitive to the noises, which caused the snake probably to converge toward themselves but not the real objective boundary.

2.2.4 Simulated Static Electric Field (SSEF) Snake

Based on the electric field's principle, the SSEF snake model was proposed [12]. Assuming an electric field was generated by many simulated static charges; therefore, the external energy function was able to be calculated by Coulomb's law via analyzing static electric field. Given an image, the gradient map of the boundary could be regarded as a charge loop, and each point on this loop was a single charge. Hence, this loop was able to generate a desired field, which should result in the total electric field being generated by the vector sum of each electric field. This field was calculated by the equation with respect to the direction, $\vec{E}=\sum_i \frac{\nabla f_i}{r^2+\varepsilon} \frac{\vec{r}}{r}$ $r \neq 0$. In this equation, ∇f_i was the ith gradient point on this loop, and r was the distance from the ith charge and ε was a constant with a small value. This energy function was regarded as the external energy function in minimizing the snake energy function of basic active contour. There were three steps in this object tracing process for SSEF snake: Edge Map Calculation and Thinning, Closed Contour Finding and Boundary Tracing with Snake. The objective boundary was able to be finally obtained through the three steps.

The SSEF snake was proposed in order to solve the imperfections in the GVF snake. If the concavity region of an objective boundary became more and more narrow form the entrance, the GVF snake was not able to converge into the narrow concavity. However, the SSEF snake was still able to generate attractive force, even a very weak force was also able to act on the snake, and caused the snake to converge toward the narrow concavity region. Additionally, the SSEF snake had more strong ability in resistance to noise than the GVF snake due to its attractive force at the objective boundary might counteract the attractive force coming from the noises. The SSEF snake was able to solve most of disadvantages coming from the GVF snake; nevertheless it still could not solve the initialization problem, which also existed in most other snakes. Snakes were influenced by the initialization position for them. If most parts of the snake had the force pointing in similar directions, the forces on the entire snake achieved an imbalance; it was hard for the snake to come to a convergence [12]. The improper initialization positions were able to cause snakes to fail.

2.3 Geometric Deformable Models

Geometric deformable models were proposed independently by Caselles and Malladi et al. [6, 7]. These models were based on the theory of curve evolution and geometric flows, and in these active contour models, the curve was propagating (deforming) by means of a velocity. Two terms were contained in the velocity as well, one related to the regularity of the curve and the other shrunk or expanded it towards the boundary. The model was given by a geometric flow based on mean curvature motion. Furthermore, the model was motivated by a curve evolution approach and not an energy minimization one. It allowed automatic changes in the topology when implemented using the level-sets based numerical algorithm [8]. These models were also introduced as a geometric alternative to snake/parametric deformable models and they provide a way to overcome the limitations of parametric deformable models.

2.3.1 Geometric Active Contour Model

This model was based on the both of the curve evolution theory and the level set theory [15]. The two-dimensional evolution curves are regarded as an implicit representation, namely zero level set $\{(x,y)|\varphi(x,y,t)=0\}$. The zero level set was embedded in the three-dimensional continuous function $z=\varphi(x,y,t)$, here the level set function $\varphi(x,y,t)$ was defined as a vector distance function of the evolution curves. The curve evolution based on level set was not to attempt to track the curve position after evolving, but was to continuously renew the level set function conforming to a rule, thereby achieving the purpose of evolving the implicit closed curve (zero level set). A differential equation had to be built to describe the evolution of the continuous surface and the zero level was attracted by the edge in the image. Therefore, the surface values had to cross the zero level when the surface crosses the edge of a given object in the image. The geometric formulation of snakes was based on Euclidean curve shrinking equation. [10, 47, 48]. This intrinsic and stable model permitted a rigorous mathematical analysis. In the process of evolving a level set function, the function always maintained being simple function and also was able to process topological changes of curve flexibly. Furthermore, the model was able to extract smooth shapes and be adapted to find several contours simultaneously. However, this model was satisfactorily executed on hard images but it was not sufficient to work on the images with discontinuous edges such as gaps. In order to solve this problem, Caselled and G. Sapiro proposed geodesic active contour model via introducing a correction term to geometric active contour model.

2.3.2 Geodesic Active Contour Model

This model [15] employed methods of analytical mechanics and Maupertuis' principle, and regarded mathematical representation as its own intrinsic property, thereby out of the parameter of dependence. Therefore, the model was considered being an essential improvement based on traditional active contours. The issue of evaluating minimum energy was transformed into searching for a geodesic curve in a Riemann space with a metric derived from the image content. Therefore, in a certain framework, boundary detection was able to be considered equivalent to finding a curve of minimal weighted length. The approach for boundary detection employed active contours, based on geodesic or local minimal distance computations. Furthermore, this geodesic active contour was represented as the zero level-set of a 3-dimensional function. The geodesic curve computation was reduced to a geometric flow that was similar to the one obtained in the curve evolution approaches in geometric active contour models [51]. However, this geodesic flow included a new component in the curve velocity, based on image information, which improved some geometric active contour models. The new velocity component was able to accurately track boundaries when the gradients suffered from large variations. Additionally, in the geodesic active contour model, the solution to the geodesic flow existed in the viscosity framework, and was unique and stable. Consistency of the model was able to cause that the geodesic curve converges to the right solution in the case of ideal objects. Despite the geodesic active contour model made a significant contribution to images with high variation in their gradients such as small gaps, it was not sufficient for the image fuzzy edge [49]. Moreover, inefficient operation on algorithm also was a main shortcoming for the model.

2.3.3 Chan–Vese Model

Active contours without edges, was proposed by Tony Chan and Luminita Vese [52], therefore, it was also called Chan-Vese model. Differencing from most of active contours models, only detecting objects with edges defined by gradients, the model was able to detect objects whose boundaries were not necessarily defined by gradient. Active contour without edges was based on curve evolution and a level set formulation of the Mumford-Shah functional [53]. In the level set formulation, a particular case of the so-called minimal partition problem, deriving from the energy minimization problem, became a "mean-curvature flow", like evolving the active contour, which would stop on the desired boundary. Moreover, a partition of the image was given into two regions, the first formed by the set of the detected objects, while the second one gave the background.

Chan-Vese model was able to detect edges both with and without gradient, and was able to automatically detect interior contours. The initial curve also did not necessarily had to start around the objects to be detected and instead could be placed anywhere in the image [52]. Furthermore, the model was no sensitive to noises; therefore, the priori processing for noise removal was unnecessary. However, this model approaches to segmentation suffered from substantial difficulties because of convex. A minimization was performed over all two-valued functions, which did not form a convex collection. As a result, the optimal minimization problem is non-convex and may have local minima. Furthermore, the level set evolution methods were able to sometimes get "stuck" at undesirable local minima.

2.4 Conclusion

A general review of important snakes and their difficulties in image processing have been given in this chapter. These difficulties should be resolved in order to increase the accuracy in further image processing, such as tracking problems. In the next chapter, a new snake is going to be proposed to resolve most of these difficulties.

Chapter 3 Charged Snake

In this chapter, a new snake named the Charged Snake is proposed. This scheme employs essentially a new external force field. This field is similar to an electric field generated by static charges [12]. Snake in this field can overcome some difficulties, such as initialization, boundary concavities and capture range problems, mentioned in the previous chapter. First, basic snake behavior and difficulty of the behavior are introduced. Next, background on electric fields in physics is presented. After that, SSEF snake model is reviewed. Finally, the electric field caused by the new charged snake is discussed.

3.1 Snake Behavior and its Difficulties

3.1.1 Basic Snake Behavior

A traditional parametric snake is represented explicitly as parameterized curves, which automatically deform over a series of iterations and conform to object contours. The snake is defined as energy-minimizing splines and deformed to minimize the energy under the influence of internal and external forces.

An active contour model is represented by a closed parametric curve $C(s) = [x(s), y(s)], s \in [0,1]$, where s represents the normalized arc length of a contour. This curve moves through the spatial domain of an image to minimize the energy function:

$$E = \int_0^1 (E_{\text{int}}(C(s)) + E_{ext}(C(s)))ds$$

$$= \int_0^1 \frac{1}{2}\left(\alpha(s)|C'(s)|^2 + \beta(s)|C''(s)|^2\right) + E_{ext}(C(s))ds \qquad (3.1)$$

where E_{int} represents the internal energy of the spline due to stretching and bending, which is particularly analyzed in the energy function (3.1); $\alpha(s)$ and $\beta(s)$ are weighting parameters that control the tension and rigidity of a snake, respectively. The first-order derivative $C'(s)$ discourages stretching and makes the model behave like an elastic band by introducing tension. The second-order derivative $C''(s)$ discourages bending by producing stiffness, which results in making the model behave like a rigid rod [23]. The external energy function E_{ext} is derived from the image, and is caused by attraction of the image, so that the external energy approaches its own minimum values at the features of interest, such as boundaries.

Increasingly, researchers have put a great deal of effort into designing the external energy E_{ext} since the internal term is hard to improve.

Minimizing the energy E for a snake must satisfy the Euler equation

$$\alpha(s)c''(s) - \beta(s)c''''(s) - \nabla E_{ext} = 0 \qquad (3.2)$$

In this equation, ∇ is a gradient operator, $\alpha(s)c''(s) - \beta(s)c''''(s)$ denotes the internal force discouraging stretching and bending, and $-\nabla E_{ext}$ denotes the external potential force pulling the snake towards the desired image contour.

3.1.2 Difficulties with Snake Behavior

Figure 3.1 shows a line drawing of a filled polygon with a concavity at the top. It also shows a sequence of curves depicting the iterative progress of a traditional snake. The snake is continuously shrinking until it converges to the object boundary [12].

Figure 3.1 Snake Behavior

There are some difficulties in the design and implementation of active contour models. In the first place, the initial contour must be close to the true boundary. Second, active contours have difficulty processing into boundary concavities [1]. Thirdly, active contours are very sensitive to noise. Fourthly, the problem of short capture range is also very important in some cases [12]. Fifthly, the main weakness comes from the difficulty in the control of the contour evolution. It does not allow the simultaneous expansion and contraction of different parts of the active regions [36].

Many snake models have appeared since the first one was proposed in the work of Kass et al. [1]. Among these snakes, the *Gradient vector flow* snake [23] was the most typical one used in the past. Later, SSEF snake was successfully achieved [12], which was the first time of employing electrostatic theory in the snake model. The two snake models will be contrasted with our own model in the experiment section.

3.2 The Electric Field

In physics, the Electric Field in a certain space is generated by static charges. An electric field exerts and acts a force on other charged objects. Here, only the static charges in 2D space are considered. At first, it is necessary to consider how the field may be generated by a charge in the space. Figure 3.2 shows an electric field of the Static charge (Only attractions are considered here) [12].

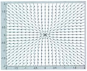

Figure 3.2 A Single Charge and its Electric Field

Based on Coulomb's Law for interacting point charge, in the static charge analysis, an electric field of a single static charge is shown [35]:

$$\bar{E} = -\frac{1}{4\pi\varepsilon_0}\frac{Q}{r^2}\frac{\bar{r}}{r} \quad r \neq 0 \tag{3.3}$$

where $\frac{1}{4\pi\varepsilon_0}$ is a constant, Q is a scalar presenting the quantity of a charge and r is the distance from the charge.

There can be more than one charge in a space, for example lots of charges located at a line, a rhombus, a double triangle (as shown in Fig.3.4.c) or an irregular shape. These fields are shown in Figure 3.3.Their original shape images without breakages are shown in Figure 3.4:

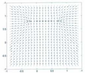

a. Line Field

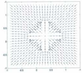

b. Rhombus Field

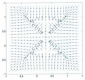

c. Double Triangle Field

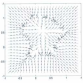

d. Irregular Field

Figure 3.3 Electric Fields for Different Cases

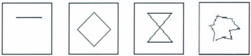

Figure 3.4 Original Images

These complex Electric Fields can also be formulated by the following Eq. (3.4):

$$\vec{E}_l = \sum_{Q} \frac{1}{4\pi\varepsilon_0} \frac{Q}{r^2} \quad \frac{\vec{r}}{r} \quad r \neq 0 \tag{3.4}$$

Certainly, at this time, the directions of E at each point in the space should be considered and Q is regarded as the each gradient point on this objective boundary.

3.3 Simulated Static Electric Field (SSEF) Snake Model

The SSEF snake model is first proposed for utilizing static electric field's principle to achieve the Snake work [1, 12]. According to the SSEF snake model, when an image is given, a gradient map for this image is going to be obtained. Based on the gradient map, then the each edge point of the image is regarded as a positive sign charge whose value equals its own pixel value. Therefore, a static electric field is generated by these charges while the electric field generates many attractions towards the edges of the image. If an initial active contour is given by a closed contour finding algorithm and the initial active contours around and close to the edges of the image, then the snake is able to be attracted towards and finally stabilize at the edges, and thus the snake work is able to be achieved by SSEF snake model. However, several main drawbacks still exist in the SSEF snake model, such as the initialization problem and difficulty in converging towards deep concave C-shape boundary. Aiming to overcome these disadvantages, a new snake model is proposed.

3.4 Charged Snake

In our work, a new snake model has been proposed via introducing a new external force employing the repulsive force created among the charges with the same sign in a certain space. The new snake consists of a set of snake points, each snake point was considered as a charge particle. All charge particles have the same magnitude and sign. The new snake model is defined as Charged Snake Model (CSM).

3.4.1 The Electric Field Created by Snake Itself

New Snake Model, CSM, can also generates an electric field in the space. In our work, only the static electric field was considered in both static charges and moving charges. To consider a charge particle in the snake, the electric field is similar to Figure 3.2 except in the opposite direction (Only repulsions are considered because of the charges with the same sign in the snake).

The electric field between two same sign charges in the CSM is showed in Figure 3.5.

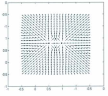

Figure 3.5 the Electric Field Generated by Two Same Charges

The following examples show lots of positive sign charges located at a round or an irregular shape. These fields are shown in Figure 3.6. And their corresponding shapes are shown in Figure 3.7, respectively.

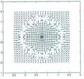

a. Round Field

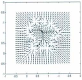

b. Irregular Field

Figure 3.6 Electric Fields for Different Cases

Figure 3.7 Original Images

These complex Electric Fields can also be formulated with the same Eq. (3.4). However, the electric fields exert action on these charges simultaneously. Each of these charges q experiences electric field force coming from other charges and these charges need to be considered separately. Therefore, the Electric Field can be formulated by the following Eq. (3.5):

$$\bar{E} = \sum_{Q \neq q} \frac{1}{4\pi\varepsilon_0} \frac{Q}{r^2} \quad \frac{\bar{r}}{r} \qquad r \neq 0 \tag{3.5}$$

Here, $\bar{E}$ is the electric field exerting on the charge q, Q is each charge in the charges group except charge q itself.

In order to make an intensive study of the CSM snake's work principle, the comprehensive electric field, the values of the charges and additional parameters in relation to the CSM snake are going to be discussed in following sections.

3.4.2 The Effect Coming from the Comprehensive Electric Fields

The electric field generated by the same sign charges has been presented before. However, our CSM snake generates an electric field itself as the snake works under another electric field generated by other opposite sign charges. Therefore, the CSM snake experiences comprehensive electric fields during its deformation towards an object boundary while the comprehensive fields come from different sign charges.

The electric field between two different signs is shown in Figure 3.8. The direction of the electric field is from positive sign charge to negative sign charge.

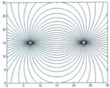

Figure 3.8 the Electric Field Generated by Two Different Sign Charges

In Figure 3.9, two examples for arbitrary amount and arbitrary sign charges are considered while the comprehensive electric fields generated by these charges are also shown as well.

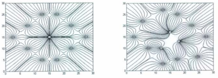

Figure 3.9 the Electric Field Generated by Arbitrary Charges

The CSM snake is continuously deformed towards the object boundary along with the chronological sequence and the snake has a great amount of charges itself, which causes the position of all the charges continuously changes. Therefore, the comprehensive electric fields are continuously changed with the continuously deformable snake based on chronological sequence. Consequently, our snake model, CSM snake, works under the situation of continuously changed electric field, which is obviously different from the other snake models.

3.4.3 The Electric Field Acting on the Snake

In our system, a snake with N positively charged particles $q_i, i = 1 \ldots N$ is considered. Based on the principle of electric fields in physics, each charge q_i in the snake moves under the influence of two forces. One force, F_c, derives from the external electrostatic field E_c generated by the interaction of the other charges in the snake. Another force, F_l, derives from another external electrostatic field E_l generated by the fixed charges, namely M negative charges e_j, $j = 1 \ldots M$. Fixed charge e_j is placed at each pixel position of the edge-map of the input image with charge magnitude equal to each edge value [29]. The approach of obtaining the edge-map of an input image will be presented in Chapter 4. The composition of two forces exerted on charges in a snake can be formulated by the following Eq. (3.6); and the composition of two electric fields exerted on charges in a snake can be formulated by the following Eq. (3.7):

$$\vec{F} = \vec{F}_c + \vec{F}_l \qquad (3.6)$$

$$\vec{E} = \vec{E}_c + \vec{E}_l \qquad (3.7)$$

Here, $\vec{F}, \vec{F}_c, \vec{F}_l, \vec{E}_c, \vec{E}_l$ can be defined as above, furthermore, $\vec{E}_c$ and $\vec{E}_l$ satisfy Eq. (3.5) and following Eq. (3.8), respectively. Therefore, Eq. (3.7) can be modified by following Eq. (3.9):

$$\vec{E}_l = \frac{1}{4\pi\varepsilon_0}\sum_{j=1}^{M}\frac{e_j}{r_j^{\,2}} \quad \frac{\vec{r}_j}{r_j} \qquad r \neq 0 \qquad (3.8)$$

$$\vec{E} = \left(\frac{1}{4\pi\varepsilon_0}\sum_{Q\neq q}\frac{Q}{r_Q^{\,2}} \quad \frac{\vec{r}_q}{r_q}\right) + \left(\frac{1}{4\pi\varepsilon_0}\sum_{j=1}^{M}\frac{e_j}{r_j^{\,2}} \quad \frac{\vec{r}_j}{r_j}\right) \qquad (3.9)$$

Our snake model works under comprehensive static electric fields, and the electric fields are generated based on the position of all positive sign charges and negative sign charges in a space. The space is a region influenced by the all charges. A snake with a large amount of positive sign charges is a continuously deformable curve based on chronological sequence till the curve fulfills the condition of energy minimization and therefore stops. Consequently, the comprehensive static electric fields in the space are continuous variation based on chronological sequence, which is different from previous snakes working under static electric fields, while the fields also influence the snake's deformation.

In the Figure 3.11, an example for the changes of the comprehensive static electric fields with a snake deforming toward the objective boundary is shown. The electric fields are continuously changed when the snake is deformed.

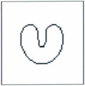

a. Original Image

b. Gradient Map

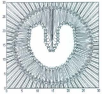

c. Initial Electric Field Base on the Changeful Snake Shape

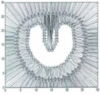

d. the Electric Field in Intermediate Process

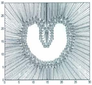

e. the Electric Field in Intermediate Process

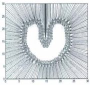

f. Final Electric Field Base on the Stable Snake Shape

Figure 3.10 Electric Fields Change with a Snake Deforming Forward the Objective Boundary

All negative sign charges, namely fixed charges, are regarded as edge points in the gradient map while all positive sign charges are regarded as snake points in the snake. Figure 3.10.c shows the initial electric fields generated by the initial snake and the objective boundary; Figure 3.10.d and Figure 3.10.e respectively show one of the intermediate processes for the electric fields change, during the deformation toward the objective boundary. Figure 3.10.f shows the final distribution for the electric fields generated by the stable snake, namely the final snake, and the objective boundary.

3.4.4 Deciding Values for the Charges in the Snake

When an image is given, the edge-map information is able to be obtained by calculating gradient map of the image. Additionally, the edge-map is obtained by applying thin method and all fixed charges are decided based on the thin edge-map information. In the thin edge map, except the interested edge information, all values in other pixel positions equal to zero. Therefore, the fixed charges for the input image are located at these non-zero pixel positions, and the quantity of each charge equals to corresponding pixel value of its own pixel position.

Furthermore, it is necessary to consider the most appropriate way to decide values of the charges in the snake. If the values are too large, the snake not only cannot be attracted towards the contour of the object, but also can be pushed too far away from the contour due to very much repulsion among the charges. As shown in figure 3.11, the snake moves towards the margin of the original image when the values of charges are too large.

Therefore, the electric field coming from the fixed charges is not sufficient for attracting the snake. If the charge values are too small, the snake can move towards the object of the input image and find out the boundary of the object. It is similar to the SSEF snake. However, there is no obvious effect for improving snake behavior as a charged snake.

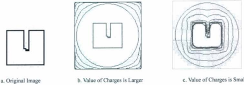

a. Original Image b. Value of Charges is Larger c. Value of Charges is Smaller

Figure 3.11 The Influence Results from Different Value of Charges in Initialized Snake

In our system, each value of the charges in the snake is the same and the value of each charge is designed as q. The value has to be determined to ensure the convergence better and faster. Hence, while the snake is initialized, the force between a fixed charge and a charge in the snake cannot be smaller than the force between two adjacent charges in the snake. When the initial snake position is located, all charges position in the snake and boundary are decided as well. The value of each charge in the snake is considered to be q, and all fixed charges are able to be obtained by thin edge-map of the original image. Therefore, the smallest force Q_s and the largest force Q_l between a fixed charge and a charge in the snake can be found by comparison. After Q_s and Q_l are found, the two distances R_s and R_l are also able to be obtained. R_s denotes the distance from Q_s to a certain charge q when the smallest force is generated by the two charges. R_l denotes the distance from Q_l to a certain charge q when the largest force is generated by the two charges as well.

Table 3.1 shows that different effects for snake deformation come from different value ranges for charges q in the snake. Consequently, comparing with other value ranges of q, when the value of q is within the range $0<|q|\le\left|\frac{r_s^2\cdot Q_s}{R_s^2}\right|$, boundary object extraction for a image is able to be obtain the best result with CSM snake.

Table 3.1 Comparison of Charges q in the Snake

	$\lvert q\rvert -> 0$	$0<\lvert q\rvert\le\left\lvert\frac{r_s^2\cdot Q_s}{R_s^2}\right\rvert$	$\left\lvert\frac{r_s^2\cdot Q_s}{R_s^2}\right\rvert<\lvert q\rvert\le\left\lvert\frac{r_s^2\cdot Q_l}{R_l^2}\right\rvert$	$\lvert q\rvert>\left\lvert\frac{r_s^2\cdot Q_l}{R_l^2}\right\rvert$
convergence	successful	successful	most of result is successful	unsuccessful
boundary concavity	good	best	better	fault
convergence speed	faster	fastest	slower	meaningless
result	similar to SSEF snake	better CSM snake	unsure deforming for CSM snake	hopeless situation

In figure 3.12, for its object original image in figure 3.11, active contour from an initial circularity moving towards the object boundary with CSM snake is shown. Here, each charge q in the initial snake is $|q| = \left|\frac{Q_s}{R_s^{\ 2}}\right|$. Furthermore, the final result of object boundary extraction is satisfactory.

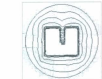

Figure 3.12 Appropriate Values of Charges in Initialized Snake

Furthermore, in our work, two additional parameters are brought to the equation for the external force of the snake model.

3.4.5 Additional Parameters for Improving Snake Behaviors

In the evolution of Snake model, external forces play a significantly decisive role. Therefore, studying and developing the external force become a significant aspect in the research on the snake model. The external field of the snake model defined by Multiscale Gaussian potential force, $E_{ext}^{(2)}(x, y) = -\left|grad(G_\sigma(x, y) * I(x, y))\right|^2$, is based on the image gradient. Thereby the model causes more difficulties in capture range, converging into the concavity, and sensitivity in initialization. Although these difficulties can be conquered by

GVF Snake Model [23], a new disadvantage, the large computation cost for solving partial differentiation, is inevitable. The conflict between computational efficiency and performance can be resolved by stimulated static electric field (SSEF) snake [28].

However, SSEF Snake Model is unable to form C-shape concavity convergence. A new external force field (virtual electrical field) can be obtained via adding two parameters h and d [28]. The new force field can be formulated by the following Eq. (3.10).

$$\bar{E}_l = \sum_{Q} \frac{1}{4\pi\varepsilon_0} \frac{Q}{(r+d)^h} \quad \frac{\vec{r}}{r} \quad r \neq 0 \tag{3.10}$$

Eq. (3.10) is derived from Eq. (3.4), In Eq.(3.4) the constant factor d is added to the distance parameter r, which therefore creates a smooth effect on the result of the snake. Simultaneously, an adjustable parameter h is introduced instead of constant power 2. Next, influences coming from the parameters d and h are presented, respectively. Hence, the new modified electrical field is not a real electrical field. It is defined as Virtual Electrical Field.

3.4.5.1 Analysis of parameter *d*

If only parameter d is considered to affect the external forces acting on a deformable snake, another parameter h should be considered as a constant. Moreover, because the external force field is in directly proportional to the variation of $\frac{1}{(r+d)^h}$ in Eq. (3.10), the variation of $\frac{1}{(r+d)^h}$ is considered instead of the external forces. In the figure 3.13, the variation of $\frac{1}{(r+d)^h}$ based on the distant parameter r is shown while the value of h is considered as constant 1.

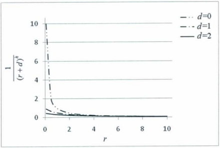

Figure 3.13 Analysis of Factor d when h Equals 1

The relation between $\frac{1}{(r+d)^h}$ and r is changed by adjusting the value of the parameter d. When d equals 0, the value of $\frac{1}{(r+d)^h}$ increases quickly as the r-coordinate approaches 0. On the other hand, as r increases the value and rate of change of $\frac{1}{(r+d)^h}$ decreases. It is evident from figure 3.13 that increasing the value of d dampens the curve's gradient making it change less under the influence of r and smoother overall. Therefore, the external forces between the deformable snake and the fixed charges near the snake are able to be decreased by increasing the value of parameter d. The purpose is to make the magnitudes of the external forces approximate the magnitudes of the other external forces between the snake and the fixed charges far from the snake. This avoids having charges in the snake that are only attracted to, and stuck on, the nearest boundary or noise but not converged towards desired object boundary.

A partial boundary of an image objective and the different partial snake shapes for the boundary are shown in figure 3.14.

(a) a Partial Boundary of an Image Objective (b) no Additional Parameter *d* (c) with Additional Parameter *d*

Figure 3.14 Different Snake Shapes Depending on the Parameter *d* for Objective Contour

The negative sign charges are considered as the objective boundary and the positive sign charges denote points in the snake shape for the boundary. The snake working without additional parameter produces a final snake contour of the boundary that is not smooth, as shown in figure 3.14(b). When some points in the snake are moved towards the boundary, the nearest snake points to the boundary points are attracted to and stick on the boundary points. Furthermore, each partial snake between two boundary points is formed into a line under the attractions coming from the two boundary points. Therefore, the final snake is deformed into a rougher shape. However, this problem is solved by introducing the additional parameter d which lets positive snake charges to deviate from their closest negative boundary neighbors. The stabilized snake is smoother, as seen in shown in figure 3.14(c).

Another significant reason to introduce the additional parameter d is to help the snake to ignore noise as it is being deformed. Normally snake points would be lock onto pixel positions of noise since the noise would be considered to be boundary points. Now the snake can pass over them because their influence is dampened as d is increased. In summary, increasing d produces smoother contour snakes with the added effect of increasing noise tolerance.

3.4.5.2 Analysis of parameter *h*

If we consider the parameter d to be constant we can see the affect that the parameter h has alone on the external forces acting on a deformable snake. In the figure 3.15, the variation of $\frac{1}{(r+d)^{h}}$ based on the distant parameter r is shown with the value of d set to zero.

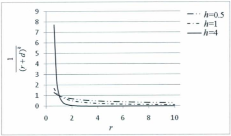

Figure 3.15 Analysis of Power h when d Equals 0

The three curves in the figure correspond to different values of parameter h. If the value of the parameter h is larger, the value of $\frac{1}{(r+d)^h}$ is smaller as r increases and larger as r decreased. The parameter h modulates overall attraction between charges. Decreasing h correspondingly decreases the attractive forces between near pairs of oppositely charged points and increases the attractive forces between far pairs of oppositely charged points.

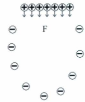

(a) Forces Acting on the Positive Sign Charges

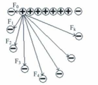

(b) Analyzing Forces Acting on a Positive Sign Charge

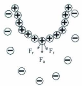

(c) Analyzing Forces Acting on a Positive Sign Charge with CSM Snake Model

Figure 3.16 Analysis of the Positive Sign Charge Moving from the Entrance of C-shaped Contour

Figure 3.16 shows a set of negative sign charges arranged in a deep concave C-shaped contour with all positive sign charges forming a line just outside it. All of positive sign charges are considered to be the snake. Furthermore, F in figure 3.16(a) denotes forces coming from all negative sign charges, and F_i in figure 3.16(b) denotes each force between a positive sign charge and each negative sign charge. In figure 3.16

(a), when the positive sign charges arrive at the entrance of the C-shape contour, each of the charges experiences all forces coming from all negative sign charges. However, any one force between the positive sign charge and a certain negative sign charge is based on the distance between the pair of charges. Moreover, the attraction between the positive sign charge and its near negative sign charge is more than any attraction generating by those negative sign charges far away from the positive sign charge. Therefore, if a positive sign charge is located near the entrance of the C-shape contour, the charge will be attracted toward the negative sign charge closest to entrance, and then stays at the entrance. In other words, such a snake with only positive sign charges has difficultly entering through the entrance of a C-shape region, thereby failing to converge toward a deep concave contour. However, this problem is able to be solved via adjusting parameter *h*. As figure 3.16 (b) shows, the first positive sign charge on the left is analyzed. The charge experiences the forces coming from all negative charges. Also, the distance between the positive charge and the negative charge at the entrance is much nearer than others, namely, F_0 is much larger than other forces. The charge therefore is going to stick on the negative and not move towards other negative sign charges. However, parameter *h* is able to be adjusted to obtain $\sum_{i=1}^{k} \bar{F}_i \geq \bar{F}_0$. Therefore, the external forces coming from far negative sign charges and acting on a snake are increased; as a result, the snake is able to extricate itself from near external forces and deform towards the far objective boundary as well. The positive sign charge is able to go through the entrance of the C-shape region and be attracted towards the deep concave boundary. Our CSM snake not only attracts but also repels when deforming. As figure 3.16 (c) shows, aiming to a certain positive sign charge in the snake, F_r denotes repulsions coming from other charges in the snake while F_a denotes attractions coming from object boundaries. The force both F_r and F_a are in the deep concavity boundary directions. The charge is able to move towards the object boundary with the snake deforming and finally arrive at the boundary based on the condition $\vec{F}_a + \vec{F}_r \geq 0$. Therefore, in CSM snake, repulsions among charges in the snake also advance the snake deforming towards object boundary as the parameter h is adjusted.

Other positive sign charges in the snake are also able to be similarly analyzed. The snake therefore is able to converge into the inside region of C shape [28]. Consequently, the snake can be deformed into the region of C-shape with a smaller parameter value of h.

In our snake model, the virtual electric field is used to replace a simulated static electric field. Therefore, the two additional parameters can be brought into the new energy function to improve the new snake model. Our final energy function also can be improved and formulated by following Eq. (3.11) from Eq. (3.9):

$$\vec{E} = \left(\frac{1}{4\pi\varepsilon_0}\sum_{Q\neq q}\frac{Q}{r_Q{}^2} \quad \frac{\vec{r}_q}{r_q}\right) + \left(\frac{1}{4\pi\varepsilon_0} * \sum_{j=1}^{M}\frac{e_j}{(r_j+d)^h} \quad \frac{\vec{r}_j}{r_j}\right) \tag{3.11}$$

Furthermore, the given formula could be modified and improved so that our snake model can be better implemented towards the desired result of the object contour for an image. As shown in Eq. (3.11), two additional parameters are employed in the given formula for obtaining the virtual electric field in our CSM snake model. A few examples proving the effects are shown in figure 3.17. These figures show the effects of using the CSM snake with a variation of d as the value of h equals 1 and with a variation of h as the value of d equals 2, respectively.

a. Original Image

d=0			
d=1	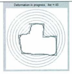	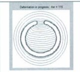	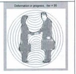

d=2	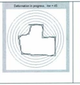	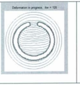	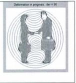

b. as the Value of *h* Equals 1

h=0.5	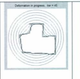	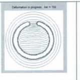	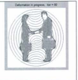
h=2	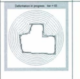	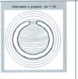	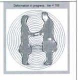
h=4	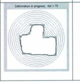	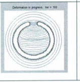	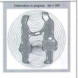

c. as the Value of *d* Equals 2

Figure 3.17 the Work Effects Using the CSM Snake with the Variation of Parameters *d* and *h*, Respectively

The effects of achieving the CSM snake via adjusting the two additional parameters are presented in Figure 3.17. If the value of d is greater, the result of the snake is smoother. Simultaneously, the contour of the snake can be deformed into the region of a deep concave C-shape with a smaller value of h. However, the values of h and d should be properly adjusted since the convergence speed is lowered as d is increased.

The experiments using the approach will be presented in the experiment section in Chapter 5. Also, there are many more experiment results in Appendix A. In the next chapter, how the snake is used to trace the object information will be explained.

Chapter 4 Object Boundary Tracing with CSM Snake

4.1 Introduction

Normally, the CSM Snake is used to trace the more precise object information such as shape so that the object contour can return to users and provide the necessary information to the future works. This process includes two primary steps and each step is presented in detail in this chapter.

4.2 Tracing Process

In this thesis, two steps included in this object tracing process are Edge Map Calculation and Thinning, and Boundary Tracing with Snake, respectively.

4.2.1 Edge Map

The tracing process starts by calculating the Edge Map of the given image, and the Edge Map is formed by pixels where there are abrupt variations of gray levels. The variation is usually computed by the gradient of pixels. Supposing $f(x,y)$ presents an edge map

$$f(x,y) = |grad(I(x,y))|^2 \qquad (4.1)$$

where $grad()$ is a gradient operator and $I(x,y)$ is a given image.

After that, a thinning algorithm [20] is used in extracting edge map. By the thinning algorithm, noises in the edge map are able to be reduced, unreal edge information coming from gradient operation is restrained and only significant thin edge is preserved [57]. After the edge map is thinned, the amounts of fixed charges on the edge map can be significantly reduced; thereby improving computing efficiency greatly when the snake deforms towards certain image boundaries [32].

4.2.2 Boundary Tracing with CSM Snake—Numerical Solution

CSM snake model is not sensitive to the initial position. However, in order to execute snake work efficiently, an initial active contour around the object is given by a closed contour finding algorithm [55, 56]. From the initial position, the CSM snake moves closer and closer to the real boundary of object. Although the movement seems to be a quite simple visual process, there is essentially a complex computation supporting the continuous change.

A numerical solution of snake implementation mathematically demonstrates how the snake moves under the control of external forces (forces in electric field).

The snake model is a mapping:

$$[0,1] \rightarrow R^2$$

$$s \mapsto v(s) = (x(s), y(s))$$

If $F(v)$ is the external force, the following equation should be satisfied.

$$\alpha(s)v''(s) - \beta(s)v''''(s) - F(v) = 0 \qquad (4.4)$$

where $\alpha(s)$ is the tension parameter and $\beta(s)$ is the rigidity parameter.

To find a solution to Eq. (4.4), the snake is made dynamic by treating $v(s)$ as a function of time t as well as s, i.e. $v(s,t)$. The partial derivative of v with respect to t is then set equal to the left-hand side of Eq. (4.4) as follows:

$$\gamma \frac{\partial v}{\partial t} = \alpha(s) v''(s) - \beta(s) v''''(s) - F(v) \qquad (4.5)$$

The coefficient γ is introduced to make the units on the left side consistent with the right side, namely make the final system of units on the left side is also the units of force. When the solution $v(s,t)$ stabilizes, the left side is zero. A solution of Eq. (4.4) is achieved. Thus, the minimization is solved by placing an initial contour on the image domain and allowing the contour to deform according to Eq. (4.5).

Assuming there are N discrete points on the snake, thereby a step $h = 1/(N-1)$ is obtained. By approximating the derivatives in Eq. (4.5) with finite differences, and converting to vector notation $v_i^n = (x_i^n, y_i^n) = (x(ih, n\Delta t), y(ih, n\Delta t))$, Eq. (4.5) becomes:

$$\begin{aligned}
&\gamma \frac{v_i^n - v_i^{n-1}}{\Delta t} = \frac{1}{h}\left(-a_i\left(v_i^n - v_{i-1}^n\right) + a_{i+1}\left(v_{i+1}^n - v_i^n\right)\right) \\
&-\frac{b_{i-1}}{h^2}\left(v_{i-2}^n - 2v_{i-1}^n + v_i^n\right) + 2\frac{b_i}{h^2}\left(v_{i-1}^n - 2v_i^n + v_{i+1}^n\right) \qquad (4.6) \\
&-\frac{b_{i+1}}{h^2}\left(v_{i+2}^n - 2v_{i+1}^n + v_i^n\right) - F\left(v_i^{n-1}\right) \qquad i = 0 \ldots N-1
\end{aligned}$$

where $v_i = v(ih)$; $\quad a_i = \dfrac{\alpha(ih)}{h}$; $\quad b_i = \dfrac{\beta(ih)}{h^2}$. are defined, h the step size in space, and Δt the step size in time.

Eq. (4.6) can be written in the matrix form:

$$\frac{v^n - v^{n-1}}{\tau} = Av^n - F\left(v^{n-1}\right) \tag{4.7}$$

where $\tau = \Delta t / \gamma$, $v^n, v^{n-1}, and \quad F\left(v^{n-1}\right)$ are $N \times 2$ matrices, and A is an $N \times N$ matrix.

$$A = \begin{bmatrix} l_0 & m_0 & n_0 & & & & & n_{N-2} & m_{N-1} \\ m_0 & l_1 & m_1 & n_1 & & & & & n_{N-1} \\ n_0 & m_1 & l_2 & m_2 & n_2 & & & & \\ & n_1 & m_2 & l_3 & m_3 & n_3 & & & \\ & & \ddots & \ddots & \ddots & \ddots & \ddots & & \\ & & & n_{N-5} & m_{N-4} & l_{N-3} & m_{N-3} & n_{N-3} & \\ n_{N-2} & & & & n_{N-4} & m_{N-3} & l_{N-2} & m_{N-2} & \\ m_{N-1} & n_{N-1} & & & & n_{N-3} & m_{N-2} & l_{N-1} & \end{bmatrix}$$

where

$$\begin{aligned} l_i &= -(\alpha_i + \alpha_{i+1})/h^2 - (\beta_{i-1} + 4\beta_i + \beta_{i+1})/h^4, \\ m_i &= \alpha_{i+1}/h^2 + 2(\beta_i + \beta_{i+1})/h^4, \\ n_i &= -\beta_{i+1}/h^4, \\ \alpha_i &= \alpha(ih), \quad \beta_i = \beta(ih) \end{aligned}$$

Note that the snake is a closed contour, therefore the point v_N actually is v_0. Generally, $v_p = v_k \quad if \quad p(\text{mod})N = k \quad k = 0 \ldots N-1$.

Eq. (4.7) can then be solved iteratively by matrix inversion using the following equation:

$$v^n = \left(I_d + \tau A\right)^{-1}\left[v^{n-1} - \tau F\left(v^{n-1}\right)\right] \tag{4.8}$$

It is necessary to consider forces, namely $F\left(v^{n-1}\right)$ in Eq. (4.8), based on variational static electric fields while the snake deforms toward the objective boundary. $F\left(v^{n-1}\right)$

denotes the external forces acting on the snake at the time of n-1 times Δt. The forces is $N \times 2$ matrices,

$$F\left(v^{n-1}\right)=\begin{bmatrix} F\left(v^{n-1}\right)_x^0 & F\left(v^{n-1}\right)_y^0 \\ F\left(v^{n-1}\right)_x^1 & F\left(v^{n-1}\right)_y^1 \\ \vdots & \vdots \\ \vdots & \vdots \\ F\left(v^{n-1}\right)_x^{N-2} & F\left(v^{n-1}\right)_y^{N-2} \\ F\left(v^{n-1}\right)_x^{N-1} & F\left(v^{n-1}\right)_y^{N-1} \end{bmatrix}$$

$F\left(v^{n-1}\right)_j^i$ denotes the forces acting on the point i in the snake, and the forces come from j-coordinate direction of the two dimension image. Moreover, each value in the matrix is the composition of forces coming from attraction or repulsion in the coordinate direction.

If considering the whole process of a snake deformation, the static electric fields acting on the snake are continuous change base on the changeful snake shape following time order. However, each positive sign charge v_i in the snake is solely considered at a certain time point here. Assuming the snake deforms experiencing j times Δt based on time, then the forces exerting on the point v_0, namely v_0^j, is firstly considered. Because Δt is a very short interval of time, the forces acting on the point v_0 are able to be considered being changeless while points form v_1 to v_{n-1} are considered being motionless during the point v_0 changes from v_0^j to v_0^{j+1}, namely within each very short interval of time Δt. After that, forces acting on points form v_1 to v_{n-1} are alike obtained during the very short interval of time Δt, respectively. Therefore, forces acting on each snake point with positive sign charge are able to be employed in Eq. 4.8. Furthermore, in Eq. 4.8, I_d denotes the identity matrix.

Thus, a linear system is obtained and a diagonal banded symmetric positive system has to be solved. The solution is computed using a LU decomposition [33] of $I_d + \tau A$. The decomposition need be computed only once if the α, β remain constant through time ($\alpha = 0.05$ and $\beta = 0.05$ make snake best performance in this thesis). Iterations are stopped when the difference between iterations is small enough.

Normally, after some iterations the snake stops its movement and is attached to the object boundary. However, the disadvantage of this numerical solution is its time-consuming matrix computation, especially the inverse matrix calculation. A more effective algorithm should be found in the future.

4.3 Discussions

In this chapter, an entire tracing process with the snake has been demonstrated. Each supporting step in the whole process plays an important role. As for the snake tracing based on these supporting steps, after the entire tracking process is finalized, the image object shape results are finally found out. However, numerical implementation method is a crucial problem and it greatly affects the tracing efficiency. A better solution is expected for this reason.

Chapter 5 Experiments

5.1 Introduction

In this chapter, comparative results among GVF snake, SSEF snake and our CSM snake in various images are shown. Comparisons among the three snake models are considered in the following aspects: convergence into the concavity, capture range, noise sensitivity, snake initialization and convergence speed. The advantages and disadvantages for each model therefore are presented. Furthermore, several examples experimenting on complex images are shown.

5.2 Comparisons with GVF and SSEF

5.2.1 Convergence to Boundary Concavity

In the experiment, all of the CSM, the SSEF and the GVF snakes can progress into the U-shaped object. However, when the opening of the concavity becomes narrower and narrower, the GVF snake faces difficulty converging into the concavity, while both the CSM and the SSEF snake can still enter it. Figure 5.1 shows an example for narrow concavity, in which the GVF snake fails while both the CSM and the SSEF snakes succeed.

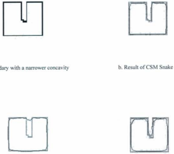

a. Boundary with a narrower concavity

b. Result of CSM Snake

c. Result of GVF Snake.

d. Result of SSEF Snake

Figure 5.1 Boundary Concavity Problems

For C-shape concavity, both the GVF and the SSEF snakes fail, however the CSM snake succeeds. (See Figure 5.2)

a. Boundary with a C-shape Concavity

b. Result of CSM Snake

c. Result of GVF Snake.

d. Result of SSEF Snake

Figure 5.2 C-shape Concavity Convergence Problem

5.2.2 Capture Range

Figure 5.3 shows the streamlines of Figure 5.1, while Figure 5.4 shows the streamlines of Figure 5.2, with the CSM snake, the SSEF snake and the GVF snake. Obviously, all schemes have a wide capture range because in Figures 5.3 and 5.4 the streamlines of these three fields extend very far away from the boundary.

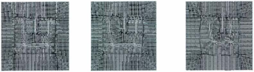

a. Streamlines of CSM; b. Streamlines of SSEF. c. Streamlines of GVF.

Figure 5.3 Comparison by Fields for the Narrower Concavity

a. Streamlines of CSM; b. Streamlines of SSEF. c. Streamlines of GVF.

Figure 5.4 Comparison by Fields for the C-shape Concavity

5.2.3 Noise Sensitivity

In the experiment, noise is introduced. Figure 5.5 shows the original noised image and results from the CSM, the SSEF and the GVF snakes.

GVF snake is very sensitive to the noise because the snake adheres to the noise while both the SSEF snake and the CSM snake are much less sensitive to it. The insensitivity of both the SSEF snake and the CSM snake is due to forces from the boundary counteracting the forces created by each noise point. Hence, SSEF and CSM snakes will not adhere to the noise easily.

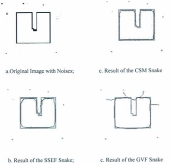

Figure 5.5 Comparison among CSM Snake, SSEF Snake with GVF Snake for Noisy Image

5.2.4 Initialization Position for the Snake

The snake initialization problem is similar on both the SSEF snake and the GVF snake due to employing a force field as their external force [12]. If most parts of the snake have the force pointing in similar directions, the forces on the entire snake achieve an imbalance; it is hard for this snake to come to a convergence [12]. Figure 5.6 shows one of the improper initialization positions that can cause both snakes to fail.

a. In the SSEF Snake; c. In the GVF Snake

Figure 5.6 Improper Initializations in Both the SSEF Snake and the GVF Snake

However, the initialization problem can be conquered in the CSM snake because of the existing external force, repulsion among same sign charges, generated by charges in the snake self. Therefore, the problem of convergence toward a partial object, brought from the snake's initialization position, may be successfully overcome. Figure 5.7 shows that for the improper initialization positions CSM snake can successfully achieve the object boundary.

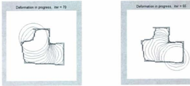

Figure 5.7 Two Improper Initializations in CSM Snake

5.2.5 Convergence Speed

The efficiency of the schemes is tested mainly by taking the iterations in dynamic computation into account because this computation is the most time-consuming part. The experimental data shows that the CSM snake takes only 75 iterations to convergence while the SSEF snake and the GVF snake take 90 and 110, respectively, under the same condition illustrated in Figure 5.8. Furthermore, in other cases, the CSM snake is also faster than both other snakes.

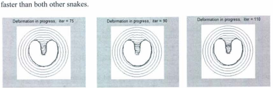

a. Iterations of CSM Snake, b. Iterations of SSEF Snake, c. Iterations of GVF Snake.

Figure 5.8 Comparison by Convergence Speed

5.4 CSM Snake in a Complex Image

All example images presented before are simple images with obvious boundary contours. However, most of real images are complex images with disconnections on contours, tiny branches attached to contours and noise as well [12]. In complex images (Figure 5.9a) , the contour is cracked and attached with small branches. Noise also appears in the edge map. Figure 5.9b shows the result of tracing with the SSEF snake. The same image is examined by CSM snake and the result as showing as Figure 5.9 c. Two more images are examined and both results are shown in Figure 5.9. Comparing between the two snakes, the SSEF snake works well in this image with only a few errors while the CSM snake works much better. More complex images are shown in Appendix A.

a. b. c.

a. b. c.

a. b. c.

a. Edge Map of a real image; b. Result after tracing with the SSEF snake; c. Result after tracing with the CSM snake

Figure 5.9 Experiments for CSM Snake

In the second set of images in Figure 5.9, there are separate three fishes in the original image. Comparing the two contour extracting results after performing SSEF snake and CSM snake respectively, the investigation of achieving image segmentation by CSM snake is able to be evidenced because the external forces acting on partial snake larger than internal tension. The external forces are repulsions among positive charges in the snake combining the attractions coming from segmented image boundaries. Therefore, the snake is disconnected and recombined as segmented snakes. Furthermore, the segmented snakes continuously deform towards their own objective boundaries result in achieving image segmentation.

5.5 Discussion

5.5.1 Sharp Corner Problem

There is a disadvantage existing in the CSM and SSEF snake. That is, the snake contour cannot stop at sharp corners when it is tracing the object boundary. The reason is that the two close lines of a sharp corner can counteract each other when the field force is computed. Therefore, the external force is too weak around the corner to stop the movement of snake. Usually, the snake is somewhat inside the sharp corner and shown as a segment of an arc.

5.5.2 Extension to 3-Dimensional (3D) Space

Since electric field exists in 3D Space, the snake field derived from it also can be extended into 3D space. But at this time, the snake is not a deformable curve but a deformable surface. Consider the surface of a sphere. Each point on this surface can be regarded as a static charge that has its field over the entire 3D space. The overall field caused by all points must be the desired field that could act as an external force in the snake energy function. The initializing a snake surface has the same appropriate charges. All of the charges have different sign and value to the charges on the object surface. So the deformable surface certainly will converge to object surface.

5.6 Summary of Contributions

In this thesis, a novel snake model, CSM, derived from the static electric field's principle in physics, is presented. In the snake model, a snake is considered to be electriferous, namely each point in the snake is considered as the same charge. All charges in the snake are subject to two external forces. One force derives from the external electrostatic field generated by interaction of the other charges in the snake; another force derives from the external electrostatic field generated by the fixed charges placed at each pixel position of the input image with quantities of electricity equal to the edge values of the input image. The two external forces acting on the snake result in the snake carrying all its own charges better moving towards the contour of the object. For instance the first force, repulsions among charges in the snake, is able to direct the snake better to adhere to the contour of the object. Furthermore, two additional parameters are employed in the special electric field formula, which can cause the snake to be attracted towards and form a deep C-shape concavity convergence via proper adjustment of the two additional parameters. Simultaneously, a series of processes are performed to the snake model. Moreover, the entire system consists of several consecutive processes, which include *Edge Map Calculation and Thinning,* and *CSM Snake Tracing*.

The snake is an independent technique that has been studied for decades. The CSM snake is a new, independent technique that is not only for object contour extraction but also be used in other image processing tasks. The CSM snake proposed in this thesis is better than other snakes proposed before in image processing since it overcomes some difficulties that appeared in the research before. Some comparisons among CSM snake, SSEF snake and GVF snake were made in this thesis. They show how the CSM snake resolves their problems.

5.7 Future Research

A conventional computation method is applied in the CSM snake design. This computation is somewhat time-consuming, which affects the speed of movement from initial status to convergence. A highly efficient method is expected to implement it. The quicker implementation indicates that the system allows the faster changes between frames. Also, such an improvement can benefit other efficiency sensitive applications of snakes. Some researchers have considered the implementation problem for a long time and have developed several different algorithms such as the Greedy algorithm [34]. However, little improvement has been obtained in other applications of snake. So far, the snake was tested only by means of the conventional algorithm.

Furthermore, the quantity of electricity for each point in the initialization snake directly influences the accuracy for contour extraction. In our model, it depends on the smallest charge magnitude, with no zero, of fixed charge. This method is better to make the snake move forward into the object contour. However, we cannot tell at this time if this method is the best one. Further research on deciding values for charges in the snake should be continued.

Bibliography

[1] M. Kass, A. Witkin and D. Terzopoulos, "Snakes: Active Contour Models", *Int. J. Computer Vision*, vol. 1, no. 4, pp. 321–331, 1987.

[2] A. Black and A. Yuille, editors. *Active Vision*. MIT Press, pp. 155-172.1993.

[3] B. Galvin, B. McCane and K. Novins, "Virtual Snakes for Occlusion Analysis", *IEEE Computer Society Conference on Computer Vision and Pattern Recognition,* Fort Collins, Colorado, vol. 2, pp. 2294, June 1999.

[4] N. Paragios and R. Deriche, "Geodesic Active Contours and Level Sets for the Detection and Tracking of Moving Objects", *IEEE Transactions on Pattern Analysis and Machine Intelligence*, vol. 22, pp. 266-280, 2000.

[5] G. A. Giraldi, L. M. Goncalves and A. F. Oliveira, "Dual Topologically Adaptable Snakes", *Proceedings of the Fifth Joint Conference on Information Sciences (JCIS'2000, Vol. 2) - Third International Conference on Computer Vision, Pattern Recognition, and Image Processing,* pp. 103-106, February, 2000.

[6] V. Caselles, R. Kimmel and G. Sappiro, "Geodesic Active Contours", *International Journal of Computer Vision*, vol. 22, pp.61-79. 1997.

[7] R. Malladi, J.A. Sethian and B.C. Vemuri, "Shape Modeling with Front Propagation: A Level Set Approach", *IEEE Transactions on Pattern Analysis and Machine Intelligence*, vol. 17, no. 2, pp. 158-175, 1995.

[8] S.J. Osher and J.A. Sethian, "Fronts Propagation with Curvature Dependent Speed: Algorithms Based on Hamilton- Jacobi Formulations", *Journal of Computational Physics*, vol. 79, pp. 12-49, 1988.

[9] L. Cohen and I. Cohen, "Finite-element Methods for Active Contour Models and Balloons for 2-D and 3-D Images", *IEEE Transactions on Pattern Analysis and Machine Intelligence*, vol. 15, no. 11, pp. 1131-1147, 1993.

[10] Sh. F. Hamidpour, A. Ahmadian, R.A. Zoroofi and J.H. Bidgoli, "Hybrid

Segmentation of Colon Boundaries in CT Images Based on Geometric Deformable Model", *IEEE International Conference on Signal Processing and Communication*, ICSPC07, 24-27 November 2007 Dubai, UAE, 2007.

[11] N. Paragios, O. Mellina-Gottardo and V. Ramesh, "Gradient Vector Flow Geometric Active Contours," *IEEE T-PAMI*, vol. 26, no. 3, pp. 402-407, 2004.

[12] D. Yuan and S.W. Lu, "Simulated Static Electric Field (SSEF) Snake for Deformable Models", *16th International Conference on Pattern Recognition (ICPR'02)*, Quebec City, Canada, vol. 1, pp. 10083, August 2002.

[13] A. Blake and M. Isard, "Active Contours", Springer-Verlag Press,1998.

[14] D. Cohen, "On Active Contour Models and Balloons", *CVGIP: Image Understanding*, vol. 53, pp. 211-218, 1991.

[15] V. Caselles, R. Kimmel and G. Sapiro, "Geodesic Active Contours", *International Journal of Computer Vision*, vol. 22, no. 1, pp. 61-79. 1997.

[16] S. Kichenassamy, A. Kumar, P. Olver, A. Tannenbaum, and A. Yezzi, "Gradient Flows and Geometric Active Contour Models", *IEEE International Conference on Computer Vision*, Boston, USA, pp. 810-815, 1995.

[17] R. Malladi, J. Sethian and B. Vemuri, "Shape Modeling with Front Propagation: A Level Set Approach", *IEEE Transactions on Pattern Analysis and Machine Intelligence*, vol. 17, pp. 158-175, 1995.

[18] M. Isard and A. Blake, "Contour Tracking by Stochastic Propagation of Conditional Density", *European Conference on Computer Vision*, Cambridge, UK, vol. 1, pp. 343-356, 1996.

[19] F. Leymarie and M. Levine, "Tracking Deformable Objects in the Plane Using an Active Contour Model", *IEEE Transactions on Pattern Analysis and Machine Intelligence*, vol. 15, pp. 617-634, 1993.

[20] J. F. Canny, "A Computational Approach to Edge Detection", *IEEE Transactions on Pattern Analysis and Machine Intelligence*, vol. 9, pp. 679-698, November 1986.

[21] D. Terzopoulos and R. Szeliski, "Tracking with Kalman Snakes", In A. Blake and A.

Yuille, editors, *Active Vision*, chapter 1, pp. 3-20. MIT Press, 1992.

[22] D. Terzopoulos and K. Fleischer, "Deformable Models", *Visual Computer*, vol. 4, no. 6, pp. 306-331, 1988.

[23] C. Xu and J. L. Prince, "Snakes, Shapes and Gradient Vector Flow", *IEEE Transactions on Image Processing*. vol. 7, pp. 359-369, 1998.

[24] D. Terzopoulos, A. Witkin and M. Kass, "Constraints on Deformable Models: recovering 3D shape and nonrigid motion", *Artificial Intelligence*, vol. 36, no. 1, pp. 91-123, 1988.

[25] R. Ronfard, "Region-based Strategies for Active Contour Models", *International Journal Computer Vision*, vol. 13, no. 2, pp. 229-251, 1994.

[26] H. Tek and B. B. Kimia, "Volumetric Segmentation of Medical Images by Three-dimensional Bubbles", *Computer Vision Image Understanding*, vol. 65, pp. 246-258, 1997.

[27] B.K.P Horn and B. Schunck, "Determining Optical Flow", *Artificial Intelligence*, vol. 17, pp. 185-203, 1981.

[28] H.K. Park and M.J. Chung. "External Force of Snake: Virtual Electric Field", *IEE Electronics Letters*, vol. 38, no. 24, pp. 1500-1502, 2002.

[29] A.C. Jalba, M.H.F Wilkinson and J.B.T.M Roerdink. "CPM: A Deformable Model for Shape Recovery and Segmentation Based on Charged Particles". *IEEE PAMI*, vol. 26, no. 10, pp. 1320-1335, 2004.

[30] M. Unser, "Texture Classification and Chansegmentation Using Wavelet Frames", *IEEE Transactions on Image Processing*, vol. 4, no. 11, pp. 1549-1560, November 1995.

[31] J. Li, J.Z. Wang and G. Wiederhold, "Classification of Textured and Non-textured Images Using Region Segmentation", *Proceedings of the Seventh International Conference on Image Processing*, Vancouver, BC, Canada, pp. 54-757, September 2000.

[32] R.C. Gonzalez and R.E. Woods, "Digital Image Processing". *Addison-Wesley, Reading*, MA. pp. 491-494, 1992.

[33] T. H. Cormen, C. E. Leiserson, R. L. Rivest and C. Stein, Introduction to Algorithms (2nd Edition), *MIT. Press,* September 2001.

[34] D. Williams and M. Shah, "A Fast Algorithm for Active Contours and Curvature Estimation", *CVGIP: IMAGE UNDERSTANDING*, vol. 55, No. 1, pp. 14-26, January 1992.

[35] F. Bueche and D. L.Wallach, *Technical Physics, Fourth Edition,* pp. 352-362, John Wiley & Sons, Inc. 1994.

[36] P. Dudek and D. L. Vilariño, "A Cellular Active Contours Algorithm Based on Region Evolution", *IEEE Int. Workshop on Cellular Neural Networks and Their Applications,* CNNA2006, pp.269–274, August 2006.

[37] Z. Hou and C. Han, "Force Field Analysis Snake: an Improved. *Parametric Active Contour Model," Pattern Recognition. Letters*, vol. 26, pp. 513-526, 2005.

[38] D. Perrin and C. Smith, "Rethinking Classical Internal Forces for Active Contour Models," *Proceedings of the IEEE Computer Society Conference on Computer Vision and Pattern Recognition*, vol. 2, pp. 615–620, 2001.

[39] W. Abd-Almageed and Christopher E. Smith, "Mixture Models for Dynamic Statistical Pressure Snakes," *IEEE International Conference on Pattern Recognition, Quebec City, Canada*, vol. 2, pp.20721, August 2002.

[40] L.-Y. Yu and C. Dyer, "Perception-Based 2D Shape Modeling by Curvature Shaping," *Visual Form,* pp. 272-282, 2001.

[41] W. Abd-Almageed, S. Ramadan and C. E. Smith "Kernel Snakes: Non-parametric Active Contour Models" *IEEE International Conference on Systems, Man and Cybernetics*, vol. 1, pp. 240-244, 2003.

[42] G. Giraldi, E. Straussb and A. Oliveirac, "Dual-T-Snakes Model for Medical Imaging Segmentation", *Pattern Recognition Letters*, vol. 24, no. 7, pp. 993-1003, April 2003.

[43] N. Ray and S. T. Acton, "Motion Gradient Vector Flow: An External Force for Tracking Rolling Leukocytes with Shape and Size Constrained Active Contours,"

IEEE Transactions Medical Image Analysis, vol. 23, no. 12, pp. 1466-1478, December 2004.

[44] A. R. Mansouri, D. P. Mukherjee and S. T. Acton, "Constraining Active Contour Evolution via Lie Groups of Transformation," *IEEE Transactions Image Process*, vol. 13, no. 6, pp. 853-863, June 2004.

[45] N. Paragios, O. Mellina-Gottardo and V. Ramesh, "Gradient Vector Flow Fast Geometric Active Contours," *IEEE Transactions on Pattern Analysis Machine. Intelligence*, vol. 26, no. 3, pp. 402-407, March 2004.

[46] B. Li and S. T. Acton, "Vector Field Convolution for Image Segmentation Using Snakes," *IEEE International Conference on Image Processing*, pp. 1637, 2006.

[47] C. Xu, D.L. Pham and J.L. Prince, "Image Segmentation Using Deformable Models", *Handbook of Medical Imaging*, vol. 2, chapter 3, pp. 447-514, SPIE Press, 2000.

[48] V. Caselles, F. Catte, T. Coll et. al., "A Geometric Model for Active Contours in Image Processing", *International Journal of Computer Vision*, vol. 22, pp. 61-79,1997.

[49] H. Liu, Y. Chen, H. ho and P. Shi, "Geodesic Active Contours with Adaptive Neighboring Influence", *MICCAI(2)*, pp:741-748, 2005.

[50] B. Appleton and H. Talbot, "Globally Optimal Geodesic Active Contours", *Journal of Mathematical Imaging and Vision*, vol. 23, pp. 67-86, 2005.

[51] H. Xiao, X. Chenyang and L. P. Jerry, "A Topology Preserving Level Set Method for Geometric Deformable Models", *IEEE Transactions on PAMI*, vol. 25, no. 6, pp. 755-768, 2003.

[52]T. Chan and L. A. Vese, "Active Contours without Edges," *IEEE Transactions on Image Processing*, vol.10, pp.266-277, February. 2001.

[53] D. Mumford and J. Shah, "Optimal Approximation by Piecewise Smooth Functions and Associated Variational Problems", *Communications on Pure and Applied Mathematics*, vol. 42, pp.577-685, 1989.

[54] D. Bertsekas, "Constrained Optimization and Lagrange Multiplier Methods",

Academic Press, 1996.

[55] M. Xie and M. Thonnat, "An Algorithm for Finding Closed Curves", *Pattern Recognition Letters*, vol. 13, no. 1, pp. 73-81, January 1992.

[56] J. Hall, "PTLOC – A FORTRAN Subroutine For Determining the Position of Point Relative to a Closed Boundary", *Journal of Mathematical Geology*, vol. 7, no. 1, pp. 61-68, 1980.

[57] J. Canny, "A Computational Approach to Edge Detection", *IEEE Transactions on Pattern Analysis and Machine Intelligence*, vol. 8, no. 6, pp.679-698, 1986.

[58] R. Yang, M. Mirmehdi and X. Xie, "A Charged Active Contour based on Electrostatics", *Proceedings of the 8th International Conference on Advanced Concepts for Intelligent Vision Systems*, pp. 173-184, Springer LNCS 4179, September 2006.

[59] T. M. Deng, B.C. Lu and Y. Yu, "Automobile classification based on GVF-snake model &inertia ellipse principle", *Proceedings of the 7th World Congress on Intelligent Control and Automation*, Chongqing, China, pp. 3005 - 3008, August 2008.

[60] J. Zhang and G.Z. Wang, "Wavelet-Based Multi-scale GVF Snake Model for Image Segmentation", *IEEE Computer Society Washington*, DC, USA, Vol. 05, pp. 150-156, 2007.

[61] W.J. Niessen,B.M. ter Haar Romeny and M.A. Viergever, "Geodesic deformable models for medical image analysis ," *IEEE Transactions on Medical Imaging*, vol. 17, pp. 634 -641, 1998 .

Appendix A. Results of Images Tested with the CSM Snake and Comparisons with Both the SSEF Snake and a Traditional Snake

ID	Original Image	CSM	Boundary Tracing	Tracing Result
1				
2				
3			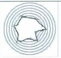	
4				
5				
6				

7				
8				
9				
10	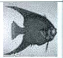			
11				
12	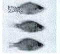			

13			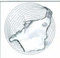	
14	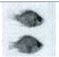			
15				
16		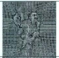		
17				
18				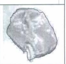

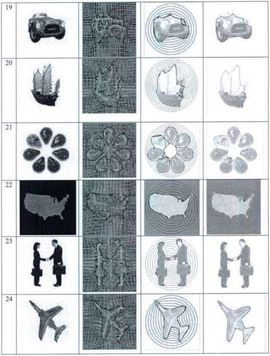
19
20
21
22
23
24

25	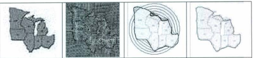
26	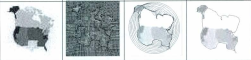
27	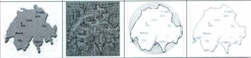
28	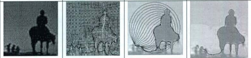
29	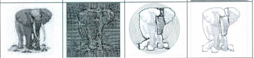
30	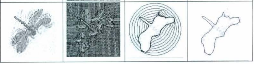

31				
32				
33				
34				
35				
36				

37				
38				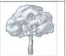
39			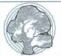	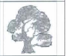
40				
41				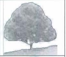
42				
43			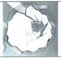	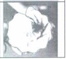

44	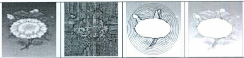
45	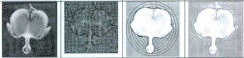
46	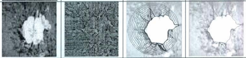
47	
48	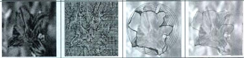
49	
50	

51	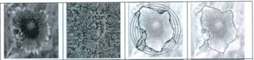
52	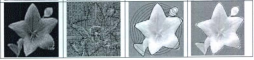

Boundary Tracing with a Traditional Snake and SSEF Snake

		SSEF Snake		Traditional Snake	
ID	Original Image	Boundary Tracing	Tracing Result	Boundary Tracing	Tracing Results
1					
2	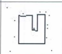			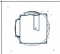	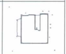
3					
4					
5		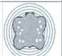			
6				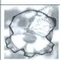	

7	
8	
9	
10	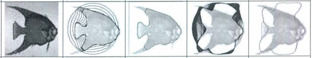
11	
12	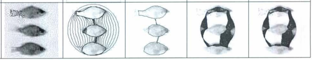

13	
14	
15	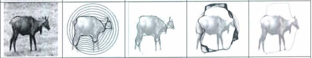
16	
17	
18	
19	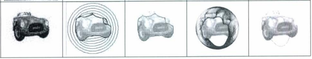

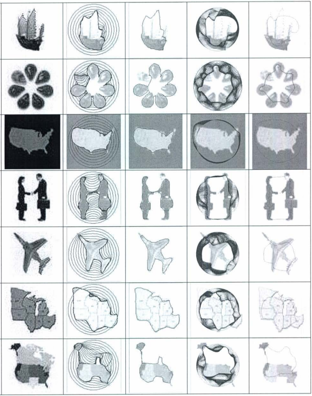
20
21
22
23
24
25
26

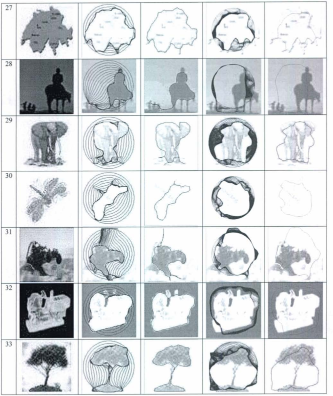
27
28
29
30
31
32
33

34	
35	
36	
37	
38	
39	
40	

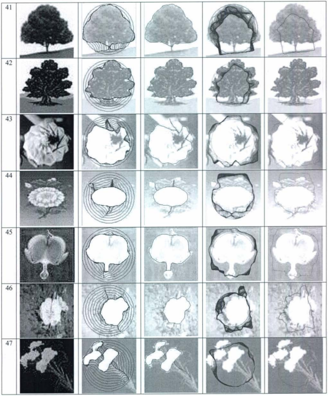
41
42
43
44
45
46
47


48
49
50
51
52

Appendix B. Comparisons of the Convergence Speed among the GVF, SSEF and CSM Snakes

Image ID	Iterations of CSM snake*	Iterations of SSEF snake*	Iterations of GVF snake*
1	40	45	65
2	90	110	145
3	40	45	75
4	30	45	160
5	35	35	85
6	120	80	140
7	50	65	50
8	60	70	40
9	55	60	90
10	50	60	95
11	40	45	85
12	80	95	80
13	60	50	70
14	110	90	55
15	90	70	95
16	40	50	80
17	55	70	85
18	25	55	75
19	40	45	75
20	80	55	70
21	90	95	70
22	40	50	90
23	85	95	45
24	50	55	120
25	45	55	75
26	60	95	90
27	70	50	75
28	100	105	115
29	150	70	55
30	40	80	60
31	65	105	70
32	60	60	65
33	75	95	110
34	75	65	45
35	90	70	145
36	35	60	105
37	45	65	65
38	40	70	70
39	30	50	55

40	50	65	65
41	45	75	80
42	50	95	85
43	95	90	50
44	85	95	70
45	35	60	100
46	80	55	65
47	85	95	70
48	90	105	75
49	100	100	60
50	60	70	65
51	60	80	125
52	40	50	65
Sum	3435	3665	4300

* 1 Unit= 5 Iterations and 1 Iteration costs 0.01 second.

The summations of the iteration show that the CSM snake is about 6.3% faster than SSEF snake while 20.1% faster than the GVF Snake. This improvement is crucial in some real-time applications.